PERGAMON

International Journal of Solids and Structures 39 (2002) 3175–3197

INTERNATIONAL JOURNAL OF SOLIDS and STRUCTURES

www.elsevier.com/locate/ijsolstr

Optimal control and optimization of functionally graded materials for thermomechanical processes

Sergio Turteltaub *

Faculty of Aerospace Engineering, Delft University of Technology, Kluyverweg 1, 2629 HS Delft, The Netherlands

Received 17 July 2001; received in revised form 27 February 2002

Abstract

The present communication is concerned with the control and/or optimization of a two-phase isotropic composite under time-dependent thermomechanical loadings. A control-like problem and a structural optimization problem are formulated using a common framework. In both cases the material properties are used as primary design variables and no a priori assumptions are made regarding the spatial distribution of each phase. For optimal control problems, the objective is to minimize the difference between field variables and target fields and for structural optimization problems the objective is to minimize the product of conjugate thermodynamical variables. Within this context, it is shown that for the minimum structural compliance problem, the optimal distribution of material properties depends on the loading history, even though the deformations are elastic. For a simplified thermal barrier design, it is shown that the problem requires simultaneous control of stresses and thermal energy via a multi-objective formulation. © 2002 Published by Elsevier Science Ltd.

Keywords: Optimal design; Functionally graded material; Inverse problem; Parameter identification

1. Introduction

The efficient use of non-homogeneous composite materials for mechanical and/or thermal applications has been one of the main thrusts behind the development of functionally graded materials (FGMs). Though many examples of such composites date back to the early developments of metallurgy, the systematic analysis within a conceptually unified framework is relatively new. The monograph of Suresh and Mortensen (1998) summarizes some of the most relevant research in the field in the last decade. Nonetheless, since this is a multi-disciplinary field, a considerable body of research related to FGMs cannot be covered in a single book.

The concept of a FGM is invariably tied to an optimization problem. In particular, in order to justify the FGM, one or more qualities of the non-homogeneous composite have to be better compared to a reference

* Tel.: +31-15-2789552.
E-mail address: s.r.turteltaub@ir.tudelft.nl (S. Turteltaub).

0020-7683/02/$ - see front matter © 2002 Published by Elsevier Science Ltd.
PII: S0020-7683(02)00243-3

homogeneous composite. In this regard, the concept of (material) topology optimization is particularly suitable for designing FGMs. The monographs of Bendsøe (1995) and Cherkaev (1999) summarize the mathematical and computational aspects of optimization of material properties.

Related to optimization, the theory of optimal control can also be used for designing FGMs. However, as opposed to the classical framework of control—in which the external loading is viewed as the control variable—the material properties are used as design variables for FGMs whereas the loading is assumed to be known (and not controllable). Consequently, optimal control using variable material properties is a non-linear problem, even if the governing equations are linear with respect to the field variables.

In the present communication, a design methodology that combines elements from topology optimization and optimal control is used to design optimal FGMs. Optimal control is incorporated in the formulation in order to model quasi-static and transient behavior, which, as shown in subsequent examples, play an important role in the optimization procedure. The time-dependent loading is important in situations where the design has to accommodate varying external conditions, which is the norm rather than the exception in practical applications. In particular, many structural elements are subjected to *cyclic* loading rather than static. Although the material properties themselves are assumed to be time independent, their optimization has to take into account time-dependent conditions.

To analyze control-like problems and structural optimization problems simultaneously, a relatively general objective functional is used. As shown below, the difference between these two formulations depends on specific weighting functions used. In both cases the material properties are viewed as variables and the terms "control" and "design" are used interchangeably.

The region Ω where the FGM will be specified is not limited to a graded interface and in general can be any simply connected three-dimensional domain. It is worth mentioning that a formulation of this type can simultaneously handle a design in which one of the materials is intended for thermal insulation whereas the other is used for mechanical performance. The advantage is that *there is no need to specify an a priori location of each material*. Rather, the procedure automatically chooses the optimal location of each constituent and mixtures of them.

The present analysis is carried out with the following assumptions: the composite being designed is assumed to be a two phase, macroscopically isotropic, constitutively linear thermoelastic material. Furthermore, the two materials are assumed to have a relatively low contrast, i.e, the ratio between the largest property and the lowest property should not be too large. This, however, is not a strong limitation for many practical applications, but it does exclude the material/void limit case. It is worth pointing out that some results obtained in the present communication apply to the anisotropic case as well. Nonetheless, the numerical implementation of the anisotropic case falls beyond the scope of this work. Other assumptions will be noted as required.

The paper is divided as follows: Section 2 contains preliminary definitions and a general formulation of the problem. In Section 3, the gradient of the objective functional is computed and the corresponding necessary optimality conditions are developed. A numerical algorithm to solve the optimization problem is summarized in Section 4. Section 5 includes a connection between the purely mechanical time-independent minimum compliance problem and the present formulation, where an optimal reinforcement of a structure is sought for a quasi-static process. Numerical examples of optimal layouts are shown for proportional and non-proportional loadings to illustrate the effect of the loading history. Section 6 includes a numerical example of a transient thermoelastic process for a simplified thermal barrier, where the stresses are to be controlled and the thermal component is to be optimized. It is shown that a multi-objective formulation involving both stresses and thermal energy is required in order to obtain a "compromise" solution. Finally, some closing remarks are included in Section 7.

2. Formulation of the problem

Preliminaries. Consider a simply connected regular domain Ω with boundary $\partial\Omega$. On the boundary, there are mechanical and thermal loads prescribed as follows: traction on $\partial\Omega_t$, displacement on $\partial\Omega_u$, heat flux on $\partial\Omega_q$ and convection on $\partial\Omega_h$. Inside the domain Ω there is an linearly elastic, heat-conducting two-phase FGM. Suppose that the effective material properties can be described as functions of the volume fraction $\omega = \omega(\boldsymbol{x})$ of one the phases in a representative volume element centered at a point $\boldsymbol{x}$. The thermomechanical material is characterized by an (effective) Helmholtz potential

$$\psi(\boldsymbol{\epsilon}, \theta) = \frac{1}{2\rho}\boldsymbol{\epsilon}\cdot\mathbf{C}\boldsymbol{\epsilon} - \frac{1}{\rho}\boldsymbol{M}\cdot\boldsymbol{\epsilon}(\theta-\theta_{\mathrm{r}}) - c\theta\log\theta/\theta_{\mathrm{r}}, \tag{1}$$

where $\boldsymbol{\epsilon}$ is the strain tensor, θ the temperature, $\mathbf{C} = \mathbf{C}(\omega(\boldsymbol{x}))$ is the elasticity tensor, $\boldsymbol{M} = \boldsymbol{M}(\omega(\boldsymbol{x}))$ the thermoelastic tensor (or stress-temperature tensor), θ_{r} a reference temperature, $\rho = \rho(\omega(\boldsymbol{x}))$ the mass density and $c = c(\omega(\boldsymbol{x}))$ is the specific heat at constant deformation. The strain is related to the displacement field $\boldsymbol{u}$ as follows: $\boldsymbol{\epsilon} = (1/2)(\nabla\boldsymbol{u} + \nabla\boldsymbol{u}^T)$. The constitutive relations are

$$\boldsymbol{\sigma} = \rho\partial\psi/\partial\boldsymbol{\epsilon} = \mathbf{C}\boldsymbol{\epsilon} - \boldsymbol{M}(\theta-\theta_{\mathrm{r}}), \qquad \eta = -\partial\psi/\partial\theta = \frac{1}{\rho}\boldsymbol{M}\cdot\boldsymbol{\epsilon} + c\left(\log\frac{\theta}{\theta_{\mathrm{r}}} + 1\right), \tag{2}$$

where $\boldsymbol{\sigma}$ is the stress tensor and η is the entropy. Additionally, it is assumed that the material follows Fourier's law for heat conduction, i.e.,

$$\boldsymbol{q} = \boldsymbol{K}\nabla\theta, \tag{3}$$

where $\boldsymbol{q}$ is the heat flux vector and $\boldsymbol{K}$ the thermal conductivity tensor (Remark: for consistency, the heat flux is defined here using the same sign convention as for stresses). In this analysis only isotropic phases and isotropic FGMs are considered, however, from the point of view of notation, it is simpler to consider a general elasticity tensor $\mathbf{C}$. Introduce the following fourth-order tensors: $\mathbf{H} = (1/3)\boldsymbol{I}\otimes\boldsymbol{I}$, $\mathbf{J} = \mathbf{I} - \mathbf{H}$, where $\boldsymbol{I}$ and $\mathbf{I}$ are the second and fourth-order (symmetric) identity tensors respectively. For the isotropic case, one has

$$\mathbf{C} = e_{\mathrm{b}}\mathbf{H} + e_{\mathrm{s}}\mathbf{J}, \quad \mathbf{D} = e_{\mathrm{b}}^{-1}\mathbf{H} + e_{\mathrm{s}}^{-1}\mathbf{J}, \quad e_{\mathrm{b}} = 3\kappa, \quad e_{\mathrm{s}} = 2\mu, \quad \boldsymbol{M} = m\boldsymbol{I}, \quad m = e_{\mathrm{b}}\alpha, \quad \boldsymbol{K} = k\boldsymbol{I},$$

where $\mathbf{D} = \mathbf{C}^{-1}$ is the compliance tensor, e_{b} and e_{s} are the distinct eigenvalues of $\mathbf{C}$, κ is the bulk modulus, μ the shear modulus, α is the coefficient of thermal expansion and k is the conductivity. For design purposes, suppose that one disposes of two homogeneous, isotropic, linear thermoelastic materials ($i = 1, 2$) with respective properties κ_i, μ_i, α_i, k_i, mass densities ρ_i and specific heats at constant deformation c_i.

In the present analysis, all properties of a FGM occupying the region Ω are macroscopically isotropic and given in terms of functions $\hat{\kappa}$, $\hat{\mu}$, $\hat{\alpha}$, $\hat{\kappa}$, $\hat{c}$ and $\hat{\rho}$, which themselves depend on $\omega = \omega(\boldsymbol{x})$ (the volume fraction of material 1 in a representative volume element). Fields and properties can be viewed as functions of time and position as well as functions of volume fraction. To avoid additional notation the functions and their values are denoted by the same letter whenever the meaning is clear by the context.

FGM model. Since the main purpose of the present communication is the optimization procedure, a relatively simple scheme is used to estimate effective properties. In particular, it is assumed that the isotropic effective properties are given as the average between the Hashin–Shtrikman–Walpole upper and lower bounds (Hashin and Shtrikman, 1963), which can provide a good approximation for two-phase composites of moderate contrast and are automatically consistent with the bounds. The model is based on the assumption that effective material properties can indeed be computed based only on knowledge of the volume fraction ω. Furthermore, it is assumed that length scales are well separated and that second order effects due to spatially varying volume fractions are *negligible* (see Drugan and Willis (1996) for non-local effects). Non-dimensional quantities and the model used in the present analysis are included in Appendix A.

Henceforth, the volume fraction of material 1 (i.e., ω) is referred to as the design variable. The type of FGM considered in this analysis is, for example, a ceramic-metal composite with *continuously varying* volume fraction. A restriction on the admissible functions ω is that they have to be *continuous* functions of $\boldsymbol{x}$.

State equations. For a given field ω, the displacement and temperature fields are interpreted as *implicit functions* of the material properties (i.e., $\boldsymbol{u} = \boldsymbol{u}(\omega)$ and $\theta = \theta(\omega)$) since they correspond to the solution to the following uncoupled, quasi-static thermoelastic process:

$$(P)\begin{cases} \operatorname{div}\boldsymbol{\sigma}(\boldsymbol{x},t) = \boldsymbol{0} & \text{in } \Omega\times(0,T],\\ \boldsymbol{\sigma}(\boldsymbol{x},t)\boldsymbol{n} = \hat{\boldsymbol{t}}(\boldsymbol{x},t) & \text{on } \partial\Omega_t\times(0,T],\\ \boldsymbol{u}(\boldsymbol{x},t) = \hat{\boldsymbol{u}}(\boldsymbol{x},t) & \text{on } \partial\Omega_u\times(0,T],\\ \operatorname{div}\boldsymbol{q}(\boldsymbol{x},t) = \rho(\boldsymbol{x})c(\boldsymbol{x})\dot{\theta}(\boldsymbol{x},t) & \text{in } \Omega\times(0,T],\\ \boldsymbol{q}(\boldsymbol{x},t)\cdot\boldsymbol{n} = \hat{q}(\boldsymbol{x},t) & \text{on } \partial\Omega_q\times(0,T],\\ \boldsymbol{q}(\boldsymbol{x},t)\cdot\boldsymbol{n} = h(\theta^{\mathrm{a}}(\boldsymbol{x},t)-\theta(\boldsymbol{x},t)) & \text{on } \partial\Omega_h\times(0,T],\\ \theta(\boldsymbol{x},0) = \theta^0(\boldsymbol{x}) & \text{in } \Omega, \end{cases}$$

where $\boldsymbol{\sigma}$ and $\boldsymbol{q}$ are given by (2) and (3), the material properties are described in Appendix A, $\boldsymbol{n}$ is the normal outward unit vector to the boundary $\partial\Omega$, $\hat{\boldsymbol{t}}$, $\hat{\boldsymbol{u}}$, $\hat{q}$ and θ^0 are given functions, θ^{a} is a known ambient temperature field and the film coefficient h is assumed to be constant (in particular, it does not depend on ω). To avoid using different symbols, the same letters are used to designate the fields when viewed as functions of position and time (for a fixed ω) as well as when they are interpreted as implicit functions of ω (i.e., for each ω there are different fields that satisfy (P)). The spatial gradient and time derivative of the temperature are always interpreted for fixed ω. The notation f_ω corresponds to the gradient of a field f interpreted as a function of ω (i.e., it measures changes in the field when different distributions of material properties are considered). The notation $:=$ is used for definitions.

Objective functional. To analyze all problems in a unified way, an objective functional J is introduced as follows:

$$J[\omega] := \frac{1}{2}\xi^{\mathrm{s}}\int_0^T\int_\Omega \mathbf{A}(\omega)(\boldsymbol{\sigma}-\check{\boldsymbol{\sigma}})\cdot(\boldsymbol{\sigma}-\check{\boldsymbol{\sigma}})\,\mathrm{d}v\,\mathrm{d}t + \frac{1}{2}\xi^{\mathrm{t}}\int_0^T\int_\Omega B(\omega)(\theta-\check{\theta})^2\,\mathrm{d}v\,\mathrm{d}t. \tag{4}$$

The prescribed functions $\check{\boldsymbol{\sigma}}$ and $\check{\theta}$ correspond to a *target evolution of the stress and temperature fields respectively* ($\check{\boldsymbol{\sigma}}$ is assumed to be *symmetric*).

The functions $\mathbf{A}$ and B are explicit functions of the volume fraction. Several possibilities can be considered for each function, in particular:

1. *Control*. For problems where the objective is to control the stress and temperature fields, then $\mathbf{A}$ can be chosen as the fourth-order identity tensor ($\mathbf{A} = \mathbf{I}$) and B can be chosen as unity ($B = 1$).
2. *Optimization*. For problems where the objective is to minimize or maximize the energy, then $\mathbf{A}$ can be chosen as the compliance (fourth order) tensor ($\mathbf{A} = \mathbf{D}$) with $\check{\boldsymbol{\sigma}} = \boldsymbol{0}$ and B can be chosen as $B = \rho c/\theta_{\mathrm{r}}$, with $\check{\theta} = 0$. In this case, $(1/2)\mathbf{A}\boldsymbol{\sigma}\cdot\boldsymbol{\sigma}$ is the stress energy and $(1/2)B\theta^2$ is a first-order approximation of the (negative) purely thermal term in the Helmholtz potential (1) for small temperature excursions about θ_{r}. Henceforth this term is referred to as the "thermal energy" and it can be interpreted as the product of conjugate thermodynamical variables $(1/2)\rho\eta\theta$ for processes at constant deformation (similar to the stress energy $(1/2)\boldsymbol{\sigma}\cdot\boldsymbol{\epsilon}$).
3. *Optimization and control*. For problems where the objective is to minimize or maximize one component of the energy while controlling another field, then one can choose $\mathbf{A} = \mathbf{D}$ and $B = 1$ to optimize the stress energy and to control the temperature or one can choose $\mathbf{A} = \mathbf{I}$ and $B = \rho c/\theta_{\mathrm{r}}$ to optimize the thermal energy and to control stresses.

Two cases are considered in the present communication. The first one is an isothermal minimum compliance problem where the objective is to maximize the stress energy. The second one is the problem of designing a thermal barrier, where the objective is to minimize the thermal energy while controlling the stresses. An example of a control-like problem can be found in Turteltaub (2002). More generally, using weighting factors that depend explicitly on the volume fraction of one material (at a specific location) can be useful, e.g., if a stress or temperature difference in a design is more critical for one of the materials than for the other.

In the definition of J, the quantities ξ^{s} and ξ^{t} are scalar factors chosen depending on the relative importance attached to each individual objective (e.g., if stress control is more important, then $\xi^{\mathrm{s}} \gg \xi^{\mathrm{t}}$). Moreover, the sign of ξ^{s} and ξ^{t} indicate whether the corresponding term is to be minimized (positive) or maximized (negative). The interval $[0, T]$ can be thought of as representing a *cyclic loading*, but otherwise it is considered to be a given design parameter.

The values of the volume fraction ω are constrained to lie in the interval $[\omega_m, \omega_M]$, with $0 \leqslant \omega_m \leqslant \omega_M \leqslant 1$. In the examples shown in subsequent sections, the "box constraints" are chosen as $\omega_m = 0$ and $\omega_M = 1$. Nonetheless, if a given manufacturing procedure is limited e.g. by the maximum local volume fraction of one material, then one can take $\omega_M < 1$.

To avoid trivial solutions, a global constraint on ω is enforced (the so-called *resource constraint*). The integral of ω over the design domain is assumed to lie below some value R, which is chosen from the outset, i.e.,

$$\int_{\Omega} \omega \, \mathrm{d}v \leqslant R. \tag{5}$$

In this case, the value R (such that $0 < R \leqslant \mathrm{vol}(\Omega)$) serves to bound the total amount of material 1 used.

Formulation of the problem. Define the design space $\mathscr{A}$ as

$$\mathscr{A} := \left\{ \omega | \omega \text{ continuous in } \Omega, \quad \omega_m \leqslant \omega \leqslant \omega_M, \quad \int_{\Omega} \omega \, \mathrm{d}v \leqslant R \right\}.$$

The objective functional J given by (4) is seen as a function of $\omega(\boldsymbol{x})$ only since the temperature field can be obtained from (P). With this interpretation, the optimization problem can be expressed as follows:

$$(\mathrm{O}) \begin{cases} \text{Find } \omega_0 \in \mathscr{A} \text{ such that} \\ J[\omega_0] \leqslant J[\omega] \qquad \forall \omega \in \mathscr{A}. \end{cases}$$

3. Gradient and first-order optimality conditions

Due to the transient behavior and the boundary conditions considered here, the governing equations are not necessarily self-adjoint, in which case the gradient of the objective functional has to be computed solving adjoint problem(s) (see Tortorelli and Haber (1989) and Dems and Mróz (1998)). In order to compute the gradient of the objective functional with respect to the design function $\omega(\boldsymbol{x})$, first augment J with the constraints $\omega_m - \omega \leqslant 0$, $\omega - \omega_M \leqslant 0$ and $\int_{\Omega} \omega \, \mathrm{d}v - R \leqslant 0$ and introduce the corresponding Lagrange multipliers $\lambda_m(\boldsymbol{x}) \geqslant 0$, $\lambda_M(\boldsymbol{x}) \geqslant 0$ and $\Lambda \geqslant 0$ as follows:

$$L[\omega, \lambda_m, \lambda_M, \Lambda] := J[\omega] + \int_{\Omega} \lambda_m(\omega_m - \omega) \, \mathrm{d}v + \int_{\Omega} \lambda_M(\omega - \omega_M) \, \mathrm{d}v + \Lambda \left(\int_{\Omega} \omega \, \mathrm{d}v - R \right). \tag{6}$$

A direct calculation using (4) and (6) shows that the first variation of L with respect to ω is formally given by

$$\delta L[\omega,\lambda_m,\lambda_M,\Lambda;\delta\omega]=\xi^{\mathrm{s}}\int_0^T\int_\Omega \mathbf{A}\boldsymbol{e}\cdot\delta\boldsymbol{\sigma}\,\mathrm{d}v\,\mathrm{d}t+\xi^{\mathrm{t}}\int_0^T\int_\Omega Be\cdot\delta\theta\,\mathrm{d}v\,\mathrm{d}t$$
$$+\frac{1}{2}\int_0^T\int_\Omega\left\{\xi^{\mathrm{s}}\mathbf{A}_\omega\boldsymbol{e}\cdot\boldsymbol{e}+\xi^{\mathrm{t}}B_\omega e^2\right\}\delta\omega\,\mathrm{d}v\,\mathrm{d}t+\int_\Omega(-\lambda_m+\lambda_M+\Lambda)\,\delta\omega\,\mathrm{d}v, \tag{7}$$

where

$$\boldsymbol{e}:=\boldsymbol{\sigma}-\check{\boldsymbol{\sigma}},\qquad e:=\theta-\check{\theta} \tag{8}$$

measure the pointwise differences (errors) between the actual fields and the target fields, and $\delta\boldsymbol{\sigma}(\boldsymbol{x},t)$ and $\delta\theta(\boldsymbol{x},t)$ measure the difference in stress and temperature fields for two different distributions of volume fraction ω_1 and ω_2 such that $\omega_2(\boldsymbol{x})=\omega_1(\boldsymbol{x})+\delta\omega(\boldsymbol{x})$. The subscript ω indicates differentiation with respect to volume fractions, i.e., $(\cdot)_\omega=\partial(\cdot)/\partial\omega$.

To actually compute the effect of varying a material layout on the performance of the FGM, one has to solve an adjoint problem with adjoint "constitutive" relations (i.e., the purpose is to compute $\delta\boldsymbol{\sigma}$ and $\delta\theta$). Let $\boldsymbol{u}^*$ be a vector-valued function, $\boldsymbol{\epsilon}^*$ and $\boldsymbol{\sigma}^*$ tensor-valued functions (assumed to be symmetric) and θ^* be a scalar-valued function defined in $\Omega\times[0,T]$.

Following the adjoint method, one can identify the adjoint problems that $\boldsymbol{u}^*$ and θ^* should satisfy, which are as follows: given a "residual strain" $\xi^{\mathrm{s}}\mathbf{A}\boldsymbol{e}(\boldsymbol{x},t)$ ($\boldsymbol{e}$ is the stress error defined above and $\xi^{\mathrm{s}}\mathbf{A}$ is the stress weighting factor in (4)) and given a "source" term $r(\boldsymbol{x},t)=\boldsymbol{\epsilon}^*(\boldsymbol{x},t)\cdot\boldsymbol{M}(\boldsymbol{x},t)+\xi^{\mathrm{t}}Be(\boldsymbol{x},t)$ (e is the temperature error defined above and $\xi^{\mathrm{t}}B$ is the thermal weighting factor) find $\boldsymbol{u}^*(\boldsymbol{x},t)$ and $\theta^*(\boldsymbol{x},t)$ such that

$$(\mathrm{P}')\begin{cases}\operatorname{div}\mathbf{C}\boldsymbol{\epsilon}^*=\mathbf{0} & \text{in } \Omega\times(T,0],\\ \boldsymbol{\epsilon}^*=\frac{1}{2}\left(\nabla\boldsymbol{u}^*+(\nabla\boldsymbol{u}^*)^T\right)-\xi^{\mathrm{s}}\mathbf{A}\boldsymbol{e} & \text{in } \Omega\times(T,0],\\ \mathbf{C}\boldsymbol{\epsilon}^*\boldsymbol{n}=\mathbf{0} & \text{on } \partial\Omega_t\times(T,0],\\ \boldsymbol{u}^*=\mathbf{0} & \text{on } \partial\Omega_u\times(T,0],\\ \operatorname{div}(\boldsymbol{K}\nabla\theta^*)+\beta\dot{\theta}^*=-r & \text{in } \Omega\times(T,0],\\ \boldsymbol{K}\nabla\theta^*\cdot\boldsymbol{n}=0 & \text{on } \partial\Omega_q\times(T,0],\\ \boldsymbol{K}\nabla\theta^*\cdot\boldsymbol{n}=-h\theta^* & \text{on } \partial\Omega_h\times(T,0],\\ \beta\theta^*(\boldsymbol{x},T)=0 & \text{in } \Omega.\end{cases}$$

Problem (P′) is solved from time $T>0$ to time 0, but it is well-posed since the sign of $\beta:=\rho c$ is positive. Observe that the "mechanical" problem actually has to be solved first (i.e., in the reversed order compared to the direct problem (P)). Solving for the adjoint strain provides the source term for the thermal problem. With this convention, one can show that

$$\xi^{\mathrm{s}}\int_0^T\int_\Omega\mathbf{A}\boldsymbol{e}\cdot\delta\boldsymbol{\sigma}\,\mathrm{d}v\,\mathrm{d}t+\xi^{\mathrm{t}}\int_0^T\int_\Omega Be\,\delta\theta\,\mathrm{d}v\,\mathrm{d}t$$
$$=-\int_0^T\int_\Omega\left(\boldsymbol{\epsilon}^*\cdot[\mathbf{C}_\omega\boldsymbol{\epsilon}-\boldsymbol{M}_\omega(\theta-\theta_{\mathrm{r}})]+\boldsymbol{K}_\omega\nabla\theta^*\cdot\nabla\theta+\beta_\omega\theta^*\dot{\theta}\right)\delta\omega\,\mathrm{d}v\,\mathrm{d}t.$$

In view of (7) and the previous relation, the first variation of L can be written as

$$\delta L[\omega,\lambda_m,\lambda_M,\Lambda;\delta\omega]=\int_\Omega L'\,\delta\omega\,\mathrm{d}v, \tag{9}$$

where the the gradient of the augmented objective functional L is [1]

$$L'=g+f-\lambda_m+\lambda_M+\Lambda, \tag{10}$$

[1] Gradient using the topology of square-integrable functions.

and the functions f (explicit gradient of J) and g (implicit gradient of J) are given by

$$f(\boldsymbol{x}) := \frac{1}{2}\xi^{\mathrm{s}}\int_0^T \mathbf{A}_\omega \boldsymbol{e}\cdot\boldsymbol{e}\,\mathrm{d}t + \frac{1}{2}\xi^{\mathrm{t}}\int_0^T B_\omega e^2\,\mathrm{d}t \tag{11}$$

and

$$g(\boldsymbol{x}) := -\int_0^T \left\{\boldsymbol{\epsilon}^*\cdot[\mathbf{C}_\omega\boldsymbol{\epsilon} - \boldsymbol{M}_\omega(\theta-\theta_{\mathrm{r}})] + \boldsymbol{K}_\omega\nabla\theta^*\cdot\nabla\theta + \beta_\omega\theta^*\dot{\theta}\right\}\mathrm{d}t. \tag{12}$$

For computational purposes, it is useful to express problem (P′) using a different terminology. In particular, the adjoint mechanical constitutive relation is $\boldsymbol{\sigma}^* = \mathbf{C}\boldsymbol{\epsilon}^* = \mathbf{C}\left(\boldsymbol{\epsilon}^*_{\mathrm{tot}} - \xi^{\mathrm{s}}\mathbf{A}\boldsymbol{e}\right)$, where the total adjoint strain is $\boldsymbol{\epsilon}^*_{\mathrm{tot}} = (1/2)\left(\nabla\boldsymbol{u}^* + (\nabla\boldsymbol{u}^*)^T\right)$. Observe that the "residual" strain is a function of time but the boundary condition on $\partial\Omega_t$ is still expressed as a traction-free surface. Another simplification is achieved by introducing the adjoint time variable $\tau := T - t$. Using τ instead of t and $\tilde{f}(\boldsymbol{x},\tau) := f(\boldsymbol{x}, T-\tau)$ for all functions in problem (P′), it can be solved from 0 to T (an equivalent formulation can be obtained using convolutions (see Tortorelli and Haber, 1989)). Hence, problem (P′) becomes

$$(\mathrm{P}'')\begin{cases}
\operatorname{div}\tilde{\boldsymbol{\sigma}}^* = \mathbf{0} & \text{in } \Omega\times(0,T],\\
\tilde{\boldsymbol{\sigma}}^* = \mathbf{C}\tilde{\boldsymbol{\epsilon}}^* \qquad \tilde{\boldsymbol{\epsilon}}^* = \left(\tilde{\boldsymbol{\epsilon}}^*_{\mathrm{tot}} - \xi^{\mathrm{s}}\mathbf{A}\tilde{\boldsymbol{e}}\right) & \text{in } \Omega\times(0,T],\\
\tilde{\boldsymbol{\epsilon}}^*_{\mathrm{tot}} = \frac{1}{2}\left(\nabla\tilde{\boldsymbol{u}}^* + (\nabla\tilde{\boldsymbol{u}}^*)^T\right) \qquad \tilde{\boldsymbol{e}} := \tilde{\boldsymbol{\sigma}} - \tilde{\tilde{\boldsymbol{\sigma}}} & \text{in } \Omega\times(0,T],\\
\tilde{\boldsymbol{\sigma}}^*\boldsymbol{n} = \mathbf{0} & \text{on } \partial\Omega_t\times(0,T],\\
\tilde{\boldsymbol{u}}^* = \mathbf{0} & \text{on } \partial\Omega_u\times(0,T],\\
\operatorname{div}(\boldsymbol{K}\nabla\tilde{\theta}^*) + \boldsymbol{M}\cdot\left(\tilde{\boldsymbol{\epsilon}}^*_{\mathrm{tot}} - \xi^{\mathrm{s}}\mathbf{A}\tilde{\boldsymbol{e}}\right) + \xi^{\mathrm{t}}B(\tilde{\theta}-\tilde{\tilde{\theta}}) = \beta\dot{\tilde{\theta}}^* & \text{in } \Omega\times(0,T],\\
\boldsymbol{K}\nabla\tilde{\theta}^*\cdot\boldsymbol{n} = 0 & \text{on } \partial\Omega_q\times(0,T],\\
\boldsymbol{K}\nabla\tilde{\theta}^*\cdot\boldsymbol{n} = -h\tilde{\theta}^* & \text{on } \partial\Omega_h\times(0,T],\\
\beta\tilde{\theta}^*(\boldsymbol{x},0) = 0 & \text{in } \Omega.
\end{cases}$$

Optimality conditions. For the optimal distribution of material properties ω_0, the optimality condition (first-order Karush-Kuhn-Tucker condition) can be expressed as

$$\begin{aligned}
&\lambda_m \geqslant 0, \quad \lambda_M \geqslant 0, \quad \Lambda \geqslant 0,\\
&\lambda_m(\omega_m - \omega_0) \leqslant 0, \qquad \lambda_M(\omega_0 - \omega_M) \leqslant 0,\\
&\Lambda\left\{\int_\Omega \omega\,\mathrm{d}v - R\right\} \leqslant 0
\end{aligned}$$

and

$$\begin{aligned}
&\text{if } \omega_0(\boldsymbol{x}) = \omega_m && \Rightarrow G(\boldsymbol{x}) + \Lambda \geqslant 0,\\
&\text{if } \omega_m < \omega_0(\boldsymbol{x}) < \omega_M && \Rightarrow G(\boldsymbol{x}) + \Lambda = 0,\\
&\text{if } \omega_0(\boldsymbol{x}) = \omega_M && \Rightarrow G(\boldsymbol{x}) + \Lambda \leqslant 0,
\end{aligned} \tag{13}$$

where $G := g + f$ is the gradient of J and g and f are given by (11) and (12). In the previous relations, all quantities are evaluated using the fields that correspond to the solutions of problems (P) and (P′) with $\omega = \omega_0$.

4. Numerical implementation

The algorithm used for the solution of problem (O) is summarized in this section. Since the design problem is non-linear, an iterative scheme is used to find a numerical approximation of the solution.

Step 1: Suppose that one has an approximation $\omega^{(n)} = \omega^{(n)}(\boldsymbol{x})$ at iteration n (the method starts with an arbitrary configuration $\omega^{(0)} = \omega^{(0)}(\boldsymbol{x})$). With $\omega^{(n)}$, all effective material properties are computed for all points $\boldsymbol{x}$ using the model for the FGM. Using these effective properties, the transient heat conduction in (P) is solved. The time-dependent temperature field is then used in the mechanical problem in (P) and the corresponding stress field is computed. Subsequently, the action of the tensor $\mathbf{A}$ on the pointwise stress error $\boldsymbol{e}(\boldsymbol{x},t) = \boldsymbol{\sigma}(\boldsymbol{x},t) - \check{\boldsymbol{\sigma}}(\boldsymbol{x},t)$ is introduced as a time-dependent residual strain in the mechanical adjoint problem in (P′). The corresponding adjoint strain field $\boldsymbol{\epsilon}^*(\boldsymbol{x},t)$ is used in conjunction with the pointwise temperature error $e(\boldsymbol{x},t) = \theta(\boldsymbol{x},t) - \check{\theta}(\boldsymbol{x},t)$ as a time-dependent source term for the adjoint thermal problem in (P′). The direct and adjoint fields are then combined in (11) and (12) to compute $g(\boldsymbol{x})$ and $f(\boldsymbol{x})$.

Step 2: an internal iterative loop is used to determine the Lagrange multipliers $\lambda_m(\boldsymbol{x})$, $\lambda_M(\boldsymbol{x})$ and Λ. With $g(\boldsymbol{x})$ and $f(\boldsymbol{x})$ fixed, estimates of $\lambda_m(\boldsymbol{x})$ and $\lambda_M(\boldsymbol{x})$ can be readily obtained from the current values of $\omega^{(n)}(\boldsymbol{x})$ and an arbitrary estimate of Λ is assumed. All this information is then combined to obtain an estimate of the gradient L' given by (10). A line search is performed to obtain a step size [2] γ. With a temporary estimate of the new distributions of volume fractions $\omega_{\text{est}}^{(n+1)}(\boldsymbol{x}) = \omega^{(n)}(\boldsymbol{x}) - \gamma L'(\boldsymbol{x})$, new Lagrange multipliers are determined such that all constraints are satisfied. The procedure is repeated until the estimate of $\omega^{(n+1)}$ is consistent with the constraints, at which point it is accepted.

Step 3: if $\left|J^{(n+1)} - J^{(n)}\right| / \left|J^{(n)}\right|$ is smaller than a prescribed tolerance, then accept $\omega^{(n+1)}(\boldsymbol{x})$ as the solution, otherwise set $n \to n+1$ and repeat steps 1 and 2.

Other aspects of the numerical implementation in the examples shown in the next sections are as follows: four-noded plane stress piecewise bilinear elements are used for space discretization in plane stress/plane heat conduction problems. Backward Euler integration is used to solve the transient problems with an adaptive scheme. The time steps are small for $t \ll 1$ in order to capture the higher frequencies. Time steps are increased as time increases. A trapezoidal rule that takes into account the adaptive scheme is used in the discrete versions of (11) and (12). A 2×2 Gaussian rule is used for all integrals in Ω. It is worth pointing out that the discretized version of the adjoint problem (P′) is slightly different than the adjoint of the discrete version of the direct problem (P). Time discretization and integration by parts do not exactly commute; essentially there is a time shift of one time step (see e.g. Carthel et al. (1994) for a similar situation in a boundary control problem).

The field ω is approximated using the same basis functions used for the field variables. Thus, ω is discretized as a *continuous* function and it is important to compute the capacity and stiffness matrices accordingly. Consequently, one cannot take immediate advantage of the systems' matrices computed in the previous iteration (which is possible to do if ω is discretized as a piecewise constant function). Nonetheless, a piecewise bilinear approximation is consistent with continuously varying material properties. In the fully discrete version, the total number of unknowns ω is equal to the total number of nodes. This numerical algorithm was implemented and several examples are shown in the next sections.

[2] Remark: one can also implement a conjugate gradient method, but for the present thermoelastic problem it is numerically costly (see Turteltaub, 2002).

5. The isothermal minimum compliance problem

5.1. Relation between the time-independent problem and the present formulation

As opposed to controls problems (in which a target field is specified and the purpose is to minimize the error), in optimization of structures a commonly prescribed goal is to minimize its structural compliance, which, equivalently, corresponds to maximize its structural stiffness (Bendsøe, 1995). The structural compliance, for a structure Ω during a quasi-static process from 0 to T, is defined as

$$J := \int_0^T \left\{ \int_\Omega \hat{\boldsymbol{b}} \cdot \boldsymbol{u} \, \mathrm{d}v + \int_{\Omega t} \hat{\boldsymbol{t}} \cdot \boldsymbol{u} \, \mathrm{d}a - \int_{\Omega u} \boldsymbol{t} \cdot \hat{\boldsymbol{u}} \, \mathrm{d}a \right\} \mathrm{d}t, \tag{14}$$

where $\hat{\boldsymbol{b}}$ is a prescribed body force, $\hat{\boldsymbol{t}}$ is a prescribed traction on part of the boundary, $\hat{\boldsymbol{u}}$ is a prescribed displacement on the complementary part of the boundary and $\boldsymbol{u}$ and $\boldsymbol{t}$ are the actual displacement and traction for the quasi-static process (observe the negative sign for the third term). Hence, from the theorem of work and energy, J has the following interpretations: if $\hat{\boldsymbol{b}} = \hat{\boldsymbol{t}} \equiv \boldsymbol{0}$ then J is the time integral of the total strain energy, if $\hat{\boldsymbol{u}} \equiv \boldsymbol{0}$ then J is the negative of the time integral of the total strain energy. The underlying idea is that for prescribed tractions and body forces, a stiffer structure *minimizes* displacements on the boundary and for prescribed boundary displacements it *maximizes* the surface tractions.

It is insightful to make a connection between the classical problem of minimum compliance (i.e., time-independent problem) and the present formulation. To this end, one can consider the isothermal case, where the temperature is equal to the reference temperature, and assume that, for the mixed problem, either the prescribed displacements are zero or the prescribed loads are zero. To cast the minimum compliance problem using the present formulation, one can choose $\mathbf{A} = \mathbf{D}$, where $\mathbf{D} = \mathbf{C}^{-1}$ is the compliance tensor and set the target function to zero, i.e., $\breve{\boldsymbol{\sigma}} = \boldsymbol{0}$. Under these conditions, the term $(1/2)\mathbf{A}\boldsymbol{e} \cdot \boldsymbol{e} = (1/2)\mathbf{D}\boldsymbol{\sigma} \cdot \boldsymbol{\sigma}$ corresponds to the stress energy density which, provided $\boldsymbol{\sigma} = \mathbf{C}\boldsymbol{\epsilon}$, coincides with the strain energy density $(1/2)\mathbf{C}\boldsymbol{\epsilon} \cdot \boldsymbol{\epsilon}$. If non-zero displacements are prescribed, then the minimum compliance problem is obtained by setting $\xi_s = -1$ (maximize stress energy) and if non-zero loads are prescribed then one has to set $\xi_s = 1$ (minimize strain energy). In both cases, a required constraint is to satisfy the displacement-based balance equations for the quasi-static process.

For the minimum structural compliance problem, the adjoint mechanical problem admits trivial solutions in terms of the direct fields. Under the foregoing assumptions (i.e., $\breve{\boldsymbol{\sigma}} = \boldsymbol{0}$, $\mathbf{A} = \mathbf{D}$), consider the following two cases: (a) suppose that the prescribed displacements $\hat{\boldsymbol{u}}$ in the direct problem (P) are zero and $\xi^s = 1$ and (b) suppose that the prescribed tractions $\hat{\boldsymbol{t}}$ and body forces $\hat{\boldsymbol{b}}$ in the direct problem (P) are zero and $\xi^s = -1$. In case (a) and in view of problem (P″), the adjoint elastic strain is zero ($\boldsymbol{\epsilon}^* = \boldsymbol{0}$), the adjoint stress is zero ($\boldsymbol{\sigma}^* = \boldsymbol{0}$), the total adjoint strain is equal to the direct strain ($\boldsymbol{\epsilon}^*_{\mathrm{tot}} = \boldsymbol{\epsilon}$) and the adjoint displacement field coincides with the direct displacement field ($\boldsymbol{u}^* = \boldsymbol{u}$). In case (b), the adjoint strain is equal to the direct strain ($\boldsymbol{\epsilon}^* = \boldsymbol{\epsilon}$), the adjoint stress is equal to the direct stress ($\boldsymbol{\sigma}^* = \boldsymbol{\sigma}$), the total adjoint strain is zero ($\boldsymbol{\epsilon}^*_{\mathrm{tot}} = \boldsymbol{0}$) and the adjoint displacement is zero ($\boldsymbol{u}^* = \boldsymbol{0}$).

Therefore, for the particular case (a), the first term of the gradient given by (12) is zero. Furthermore, since $\mathbf{CD} = \mathbf{I} \Rightarrow \mathbf{D}_\omega = -\mathbf{D}\mathbf{C}_\omega\mathbf{D}$ and in view of (11), the gradient of J is

$$G(\boldsymbol{x}) = g(\boldsymbol{x}) + f(\boldsymbol{x}) = \frac{1}{2}\int_0^T \mathbf{D}_\omega\boldsymbol{\sigma} \cdot \boldsymbol{\sigma} \, \mathrm{d}t = -\frac{1}{2}\int_0^T \mathbf{C}_\omega\boldsymbol{\epsilon} \cdot \boldsymbol{\epsilon} \, \mathrm{d}t,$$

which corresponds to the classical unconstrained gradient in the minimum compliance problem, averaged in time throughout the quasi-static process (Bendsøe, 1995).

For the particular case (b), the first term of the gradient given by (12) is $g(\boldsymbol{x}) = -\int_0^T \mathbf{C}_\omega\boldsymbol{\epsilon} \cdot \boldsymbol{\epsilon} \, \mathrm{d}t$. Furthermore, in view of (11) with $\xi^s = -1$, the gradient of J is

$$G(\boldsymbol{x}) = g(\boldsymbol{x}) + f(\boldsymbol{x}) = -\int_0^T \mathbf{C}_\omega \boldsymbol{\epsilon} \cdot \boldsymbol{\epsilon}\, \mathrm{d}t - \frac{1}{2}\int_0^T \mathbf{D}_\omega \boldsymbol{\sigma} \cdot \boldsymbol{\sigma}\, \mathrm{d}t = -\frac{1}{2}\int_0^T \mathbf{C}_\omega \boldsymbol{\epsilon} \cdot \boldsymbol{\epsilon}\, \mathrm{d}t.$$

Hence, for both cases (a) and (b), the unconstrained gradient has the same expression. However, observe that if $\mathbf{A}$ is not the compliance tensor, then this assertion is not necessarily valid.

In the classical structural optimization problem (static problem), the objective functional is based on the "final" state, hence it is independent of the loading path for an elastic deformation. However, in the present formulation, the loading history is taken into account. Thus, for *non-proportional loading*, the optimization problem is *path dependent*, despite the fact that the deformation is elastic. For *proportional loading*, where either $\hat{\boldsymbol{u}}(\mathbf{x}, t) = \alpha(t)\hat{\boldsymbol{u}}_0(\mathbf{x})$ and $\hat{\boldsymbol{t}}(\mathbf{x}, t) = \mathbf{0}$ or $\hat{\boldsymbol{t}}(\mathbf{x}, t) = \alpha(t)\hat{\boldsymbol{t}}_0(\mathbf{x})$ and $\hat{\boldsymbol{u}}(\mathbf{x}, t) = \mathbf{0}$, the classical minimum compliance problem and the present formulation are *equivalent* since, after rescaling the multipliers by a time constant, the necessary conditions (13) are the same.

5.2. Examples of optimal designs for minimum structural compliance

In what follows, four examples of optimal reinforcement in a structure are presented. The first two examples correspond to proportional loading (axial and shear) whereas the last two illustrate the effect of non-proportional loading. Suppose that one has two materials, one referred to as the reinforcement (material 1, higher principal stiffnesses) and the other as the matrix (material 2, smaller principal stiffnesses). Normalized quantities are used, as explained in Appendix A, with $\kappa_2/\kappa_1 = 0.6$ and $\mu_2/\mu_1 = 0.5$. The design variables are the local volume fractions $\omega = \omega(\boldsymbol{x})$ of material 1 (reinforcement). The body force is assumed to be zero. A non-zero displacement history is prescribed on part of the boundary while zero traction is assumed on the rest of the boundary. The goal is to find the maximum structural stiffness. The factor ξ^{s} is set to -1 to maximize the stress energy and the weighting factor $\mathbf{A}$ is the effective compliance of the two-phase composite.

The loading in each example corresponds to a prescribed displacement boundary conditions that simulates a simple deformation. A 10 cm $\times$ 10 cm square domain is chosen. The process is isothermal and plane stress conditions are assumed (see Appendix B for the case of plane stress). The left and right sides of the domain are stress-free. The bottom edge is rigidly clamped and a prescribed displacement history on the top edge is given. The first case corresponds nominally to an axial deformation and the second case to a nominal simple shear, where "nominal" in the present context means displacement of top edge relative to bottom edge. Observe, however, that the deformations are not homogeneous.

To illustrate the path dependency of the optimal layout, two other cases are considered, both corresponding to an axial to simple shear transition. The first transition corresponds to unloading in the axial direction during half of the time interval and then to simple shear during the second half. The second transition considered corresponds to a simultaneous axial unloading and simple shear during the total time interval. Even though the initial and final states are the same for both cases (for the same material distribution), the *optimal* layouts, as shown below, are different due to a distinct stress history.

The displacements of the top edge are specified as follows (total time $T = 10$ s):

1. Axial deformation:

$$\begin{cases} u_1(\boldsymbol{x}, t) = 0, \\ u_2(\boldsymbol{x}, t) = (1 - t/T) \times 10^{-3} \text{ m}. \end{cases}$$

2. Simple shear:

$$\begin{cases} u_1(\boldsymbol{x}, t) = (t/T) \times 10^{-3} \text{ m}, \\ u_2(\boldsymbol{x}, t) = 0. \end{cases}$$

3. Axial deformation followed by simple shear:

$$\text{For } 0 < t < T/2 \quad \begin{cases} u_1(\boldsymbol{x}, t) = 0, \\ u_2(\boldsymbol{x}, t) = (1 - 2t/T) \times 10^{-3} \text{ m}, \end{cases}$$

$$\text{For } T/2 < t < T \quad \begin{cases} u_1(\boldsymbol{x}, t) = 2(t/T - 1/2) \times 10^{-3} \text{ m}, \\ u_2(\boldsymbol{x}, t) = 0. \end{cases}$$

4. Simultaneous axial and shear deformations:

$$\begin{cases} u_1(\boldsymbol{x}, t) = (t/T) \times 10^{-3} \text{ m}, \\ u_2(\boldsymbol{x}, t) = (1 - t/T) \times 10^{-3} \text{ m}. \end{cases}$$

The maximum "axial" and "shear" deformations are, nominally, 1%. In all cases a normalized value of $R = 0.25$ was used (i.e., the reinforcement corresponds to a maximum of 25% of the total volume). A uniform 30×30 mesh was used and the total number of variable time steps ranged between 40 and 70 steps depending on the problem. As it is often the case with gradient-based methods, the objective functional was reduced considerably during the first iterations but subsequently a greater number of iterations are required to resolve fine details in the design.

The optimal distribution of volume fractions of material 1 (reinforcement) are shown in Figs. 1–4 for cases 1–4 respectively. The prescribed initial and final positions of the top edge are the same for cases 3 and 4. Table 1 summarizes the improvement in structural stiffness for all cases. In particular, the table lists the improvement with respect to *no* reinforcement (i.e., pure material 2) and with respect to a *uniform* reinforcement (with the same value of $R = 25\%$).

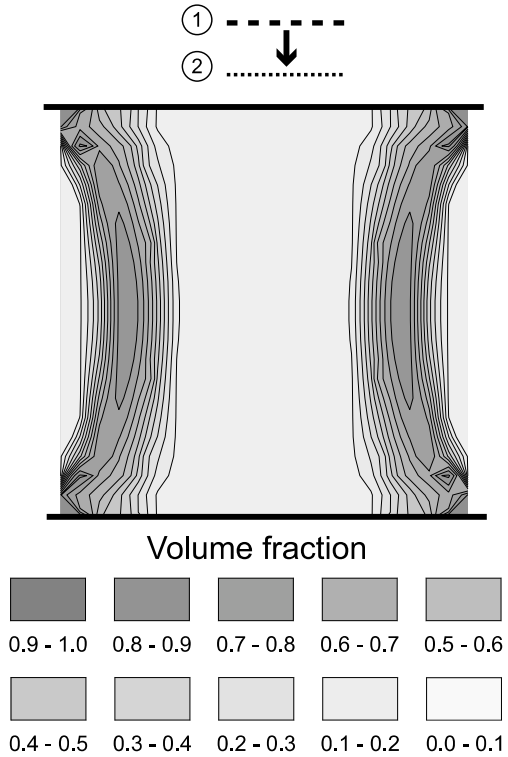

Fig. 1. Optimal distribution of volume fraction of reinforcement under prescribed axial displacement.

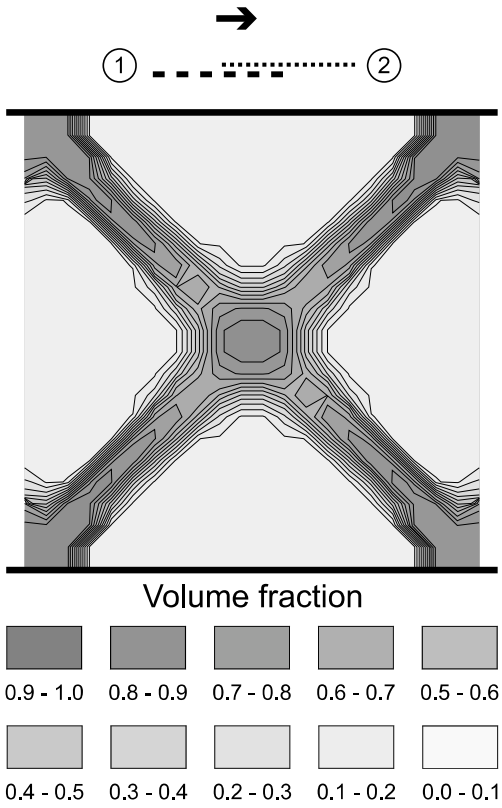

Fig. 2. Optimal distribution of volume fraction of reinforcement under prescribed simple shear.

Discussion: From Table 1 one can observe that the greatest improvement in structural stiffness using a non-uniform (graded) composite is achieved for a simple shear deformation. In the other cases a more modest but certainly non-negligible improvement is achieved. In all cases the reinforcement greatly improves the structures' stiffness compared to the non-reinforced case. For case 1 (axial-like deformation), the optimal layout is, not surprisingly, roughly a fiber-like reinforcement in the direction of the deformation. The deviation from a straight line of the fiber-like reinforcement (arched layout) is due to the stress-free sides. The reinforcement starts at the corners where the stresses are higher. For case 2 (simple shear deformation), the optimal reinforcement can be described as a truss-like internal structure with "cross-bars" rotated 45° with respect to the prescribed displacement, which again is intuitively correct. It is worth noting that in this case a graded material performs substantially better than a uniform composite. Cases 3 and 4 are more novel. Although the prescribed initial and final positions of the top edge are the same for both cases, the optimal layout depends on the displacement path. In case 3 (axial followed by simple shear), the optimal layout can be described as a single, axially oriented central fiber-like reinforcement, with additional reinforcement in each corner where the stresses reach their peak values. On the other hand, the optimal layout for case 4 (simultaneous axial and simple shear deformation) can be described as two parallel fiber-like reinforcement oriented at an angle with respect to the axial deformation. Higher reinforcement is used at the corners where, as in the other cases, the stresses are higher.

To illustrate the difference between the two designs, the computation of the objective functional for case 3 was performed using the optimal design for case 4 and vice versa. The results are summarized in Table 2.

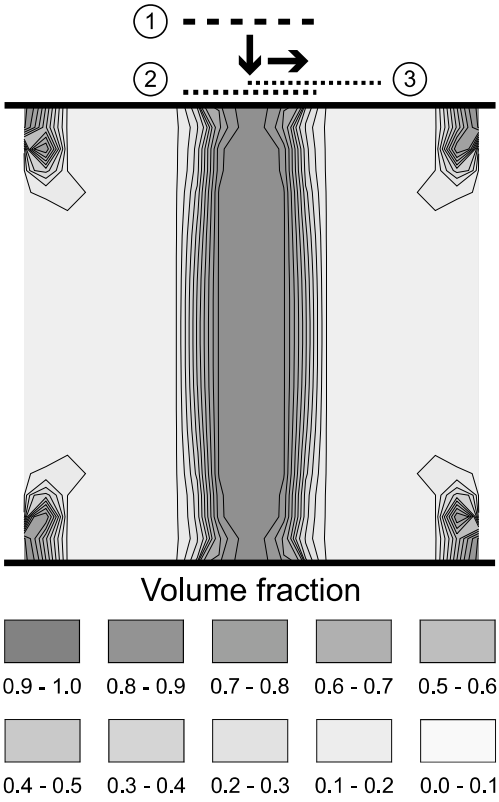

Fig. 3. Optimal distribution of volume fraction of reinforcement under axial displacement followed by simple shear.

Clearly, the optimal layout for case 3 is far from being the optimal for case 4 and vice versa. The relative improvements shown in Tables 1 and 2, quantify the importance of taking the loading history into account in order to optimize time-dependent performance.

6. Thermal barrier: multi-objective thermoelastic problem

As a second example, consider a commonly used metal/ceramic FGM system: nickel/alumina (Ni/Al_2O_3). Typically, a thin alumina coating is added on the high temperature surface to prevent damage (e.g., melting) of the metal component. Often, the coating consists of several layers with different volume fractions. With this application in mind, the foregoing example is a simplified version of a graded nickel/alumina interface. For simplicity, the formation of a thermally grown oxide layer is not considered and it is assumed that the residual stresses are zero (in general, the evolution of the microstructure is not considered in the present analysis). Nonetheless, the examples shown in this section serve to illustrate an important aspect of the optimization procedure, namely that a single objective is not enough to provide a reasonable solution. Rather, a multi-objective formulation is required. To illustrate this point, three problems are considered in this section. For all problems considered, the loading is the same, the differences are in the objective functionals used.

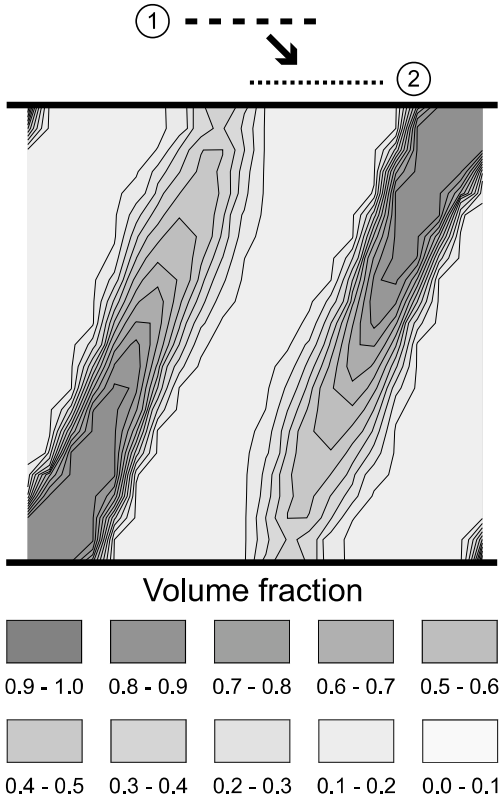

Fig. 4. Optimal distribution of volume fraction of reinforcement under simultaneous axial and shear displacements.

Table 1
Relative improvement in structural stiffness J

Nominal deformation	Improvement w.r.t. no reinforcement $(J^{opt} - J^{nr})/J^{nr}$ (%)	Improvement w.r.t. uniform reinforcement $(J^{opt} - J^{ur})/J^{ur}$ (%)
1. Axial	+65	+8
2. Simple shear	+87	+79
3. Axial plus shear	+65	+14
4. Axial and shear	+68	+16

J^{opt} is computed from (14) for the optimal reinforcement shown in Figs. 1–4; $\kappa_2/\kappa_1 = 0.6$, $\mu_2/\mu_1 = 0.5$, $R = 25\%$.

Table 2
Relative values of optimal and non-optimal structural stiffness J (computed from (14))

Nominal deformation	$(J^{opt} - J^{non\text{-}opt})/J^{non\text{-}opt}$ (%)
3. Axial plus shear	+8.5
4. Axial and shear	+11.3

The non-optimal in case 3 refers to J computed using layout 4 and, conversely, the non-optimal for case 4 is J computed using layout 3.

1. For the first problem, the purpose is to optimize the thermal energy regardless of the stresses. Hence, ξ^s is set to zero in (4) and $B = \rho c/\theta_r$.
2. For the second problem, the idea is to minimize stresses without optimizing the thermal energy. In this case, the stress weighting factor $\mathbf{A}$ is set to identity and $\xi^t = 0$ in (4).
3. The third problem consists of a multi-objective formulation where the stresses are controlled (minimized) and the thermal energy is simultaneously optimized.

Suppose that one has a 0.5 cm $\times$ 1 cm rectangular solid domain Ω. For all examples in this section, convection is prescribed on the top and bottom sides where heat is exchanged with the environment (e.g., air). Zero flux is assumed on the left and right sides. Traction-free conditions are prescribed on the top and bottom whereas zero displacement is assumed on the left and right sides. The ambient temperature is increased on the top side and left unchanged on the bottom, i.e., the thermal boundary conditions for the top and bottom sides are

$$k\nabla\theta \cdot \boldsymbol{n} = h(\theta - \theta^a),$$

where θ is the surface temperature and θ^a, the sink temperature, varies as

$$\theta^{a,top} = \theta^0 + \frac{t}{T}\theta^1, \qquad \theta^{a,bottom} = \theta^0 \quad \text{for } 0 \leqslant t \leqslant T.$$

The temperature θ^0 is a constant initial temperature larger than the reference temperature (hence, observe that initially there are non-uniform thermal stresses). In the foregoing examples, the temperatures are taken such that $\theta^0 - \theta_r = 100$ K and $\theta^1 - \theta^0 = 300$ K. The process is analyzed for $T = 10$ s.

For all problems, the domain was discretized with a uniform mesh of 30×60 (finer meshes showed convergent results). The optimal layout for problems 1–3 are shown in Figs. 5–7. In these three problems, the value of the resource constraint (maximum amount of alumina used) is $R = 25\%$. Fig. 8 corresponds to problem 3 with $R = 12.5\%$. The changes in thermal energy and stresses are summarized in Table 3 where, in all problems, the initial layout is a pure Ni domain ($\omega^0 = 0$). This initial layout is used as a reference for measuring changes in the objective functional.

Discussion. For problem 1 (thermal energy optimization, no stress control), the optimal layout consists of a one-dimensional graded interface ranging from pure alumina on the high-temperature surface to pure Ni on the lower temperature regions. From top to bottom, the concentration of alumina rapidly decreases but then changes more slowly towards a pure Ni region. The optimization of the thermal energy identifies higher temperature regions and specifies alumina in such areas. The resulting profile is a consequence of the detailed temperature distribution in both space and time. The improvement in thermal energy is about 4.7% (computed from the second term in (4) and compared to a pure Ni layout). The corresponding overall increase in stresses (not controlled in this problem) is about 32%.

For problem 2 (stress control, no thermal optimization) the optimal layout is trivially pure Ni, which corresponds to the initial layout in the iterative numerical computation. Although trivial, the solution to this problem is in fact a good illustration of several competing factors in the determination of the optimal layout. Thermal stresses arise due to several factors, namely zero-displacement boundary conditions, non-uniform distribution of temperatures and non-uniform distribution of material properties (coefficient of thermal expansion). Furthermore, reduction of thermal stresses can be accomplished via a ''global'' strategy, a ''local'' strategy or a combination of both. The term global is used here in the following sense: the use of alumina as insulation reduces the temperature inside the domain hence, in principle, reduces the thermal stresses in Ni. In this sense, the benefit of alumina is not felt where the material is, but rather at different locations. However, the trade-off is that there is a local increase of stresses due to the addition of alumina: its coefficient of thermoelasticity $m = 3\kappa\alpha$ is higher than nickel's. Thus, for the same change in temperature, at a point where the thermal expansion of the material is locally constrained, the resulting

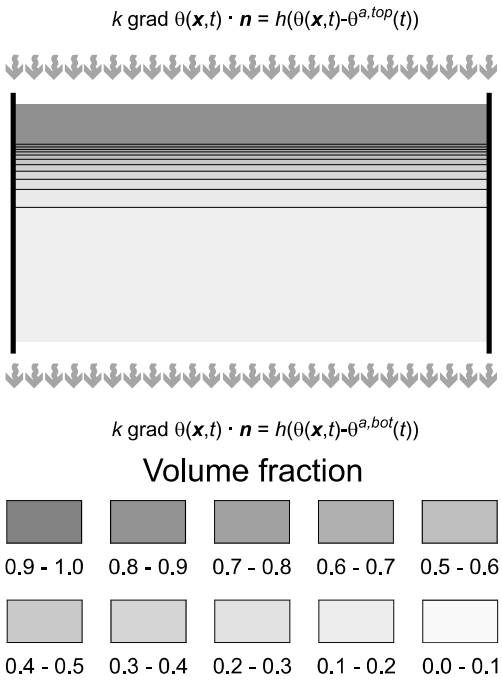

Fig. 5. Optimal distribution of volume fraction of alumina fractions for minimum thermal energy (no stress control; total time $T = 10$ s, resource $R = 25\%$).

thermal stresses would be higher for alumina than for nickel. Hence, this indicates that if one would like to locally reduce stresses, using Ni is preferable. In fact, for problem 2, this is what the computation predicts. Any addition of alumina results in an increase of thermal stresses and a reduction in temperature is not enough to offset this effect.

This second example also illustrates a simple but important fact: reduction of stresses in a FGM without consideration of the value of the temperature might easily lead to unacceptable solutions since the purpose of the coating is to prevent damage of nickel due to high temperatures. A compromise layout can be obtained between two opposite requirements: *reduce temperature in nickel without increasing thermal stresses excessively*. This formulation corresponds to problem 3, where the thermal energy is optimized and the stresses are minimized. Since the initial layout is pure Ni, the stresses would invariably increase with any addition of alumina. In this case they increase about 25%. However, the procedure prevents them from reaching an even higher value in an unconstrained optimization as in problem 1 (32%). The change in thermal energy is numerically similar to problem 1, though still slightly smaller. This is due to the actual material properties (the product $\beta = \rho c$ is similar for both Ni and alumina).

The effect of the competing factors on the optimal layout shown in Fig. 7 are particularly evident in the upper corners: the thermal stresses are higher at the corners due to the constraints (zero displacement) but the temperature is also higher due to the convection boundary conditions and a higher ambient temperature. This results in a sharper interface, which then becomes more graded farther away from the corners. This effect is still evident when the maximum amount of alumina used is reduced by half ($R = 12.5\%$), as shown in Fig. 8.

It is important to note that, due to the nature of the model used, the thermal stresses that occur due to a mismatch in coefficients of thermal expansion are only measured in an *average* (macroscopic) sense. In fact,

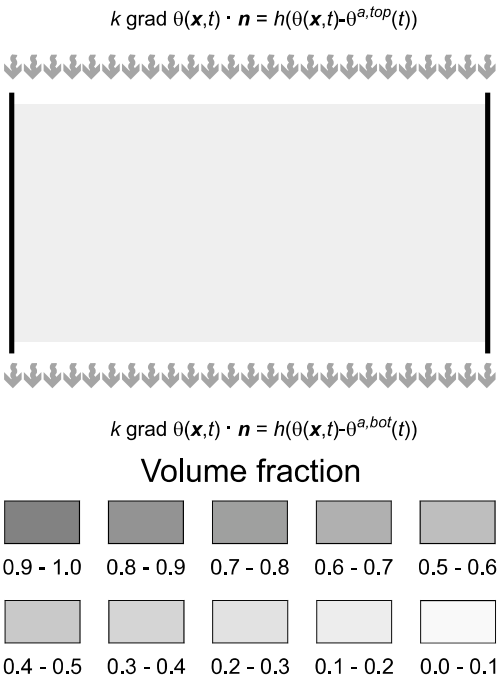

Fig. 6. Optimal distribution of volume fraction of alumina for minimum stress (no thermal control; total time $T = 10$ s). The optimal solution is trivially equal to 0 (pure Ni).

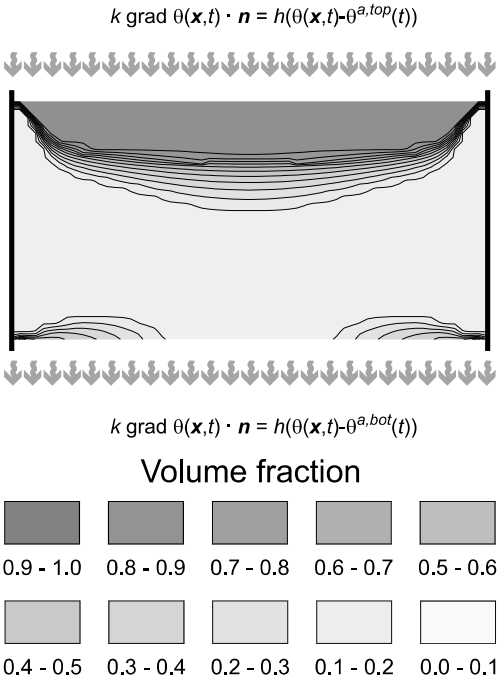

Fig. 7. Optimal distribution of volume fraction of alumina for minimum thermal energy and minimum stress (resource $R = 25\%$; total time $T = 10$ s).

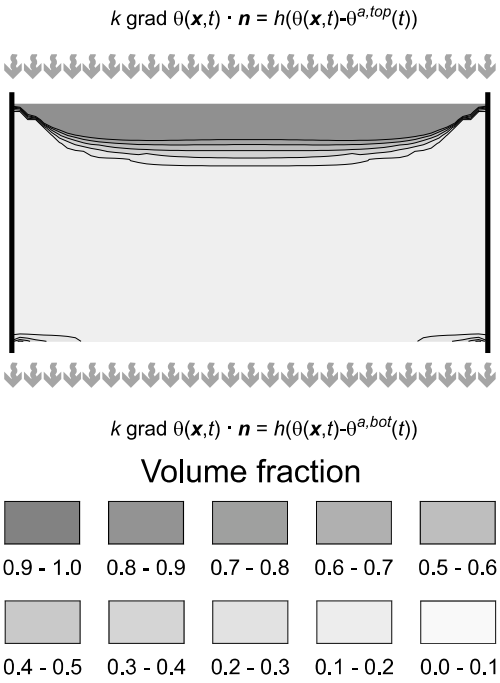

Fig. 8. Optimal distribution of volume fraction of alumina for minimum thermal energy and minimum stress (resource $R = 12.5\%$; total time $T = 10$ s).

Table 3
Relative changes in J

Objective functional	Change in stress w.r.t. no alumina $(J_{st}^{opt} - J_{st}^{0})/J_{st}^{0}$ (%)	Change in thermal energy w.r.t. no alumina $(J_{th}^{opt} - J_{th}^{0})/J_{th}^{0}$ (%)
1. Thermal optimization only	+32	+4.7
2. Stress control only	No change	No change
3. Multi-objective	+25	~+4.7

J^{opt} is computed from (14) for the optimal layouts shown in Figs. 5–7; $R \leqslant 25\%$.

the mismatch effect is typically measured at the same length scale of the thermal stresses due to *non-uniform* temperature distributions. Fluctuations of stresses inside a representative element volume are averaged and the net effect of the mismatch is only measured at a length scale large enough to reflect *changes in volume fraction*. In principle, nonetheless, one can compute the effect of inclusions at the RVE level by extending a formulation like the one proposed by Lipton (2002a) to the thermoelastic case. Such analysis, however, falls outside the present scope.

7. Closing remarks

As presented in this article, the use of optimal design and optimal control techniques can be used as a guideline for designing FGMs for average optimization and/or control purposes. The method can be applied with different material models that are based on first-order microstructural information. Furthermore,

an important advantage is that the proposed method does not require an a priori parametrization of the design space (any continuous function is admissible) nor an a priori assumption about the location of materials (as it is often the case with thermal barrier problems where pure ceramic and pure metal regions are fixed from the outset (see e.g., Tanaka et al., 1996)).

As illustrated in Section 5, the loading history is important when dealing with time-dependent objective functions and/or fields. The optimal reinforcement problem is path dependent, even though the deformation is elastic. For thermoelastic problems, as shown in Section 6, it is important to formulate the problem using a multi-objective functional.

It is worth pointing out that the local error for the minimum stress problem is an average measure in time at a given point. In particular, this means that it is possible to have two points with the same error, however one corresponds to high (peak) stress during a short time period and another to a lower stress level applied for longer time. A more sensible approach to distinguish between such cases is to incorporate a failure criterion. Since effective properties are used in the model, a homogenized failure criterion recently proposed by Lipton (2002b) can be incorporated into the formulation of the problem.

In closing, it is worth mentioning that even though current manufacturing techniques might not be able to reproduce the details of the designs presented here, the proposed numerical method can still be used as a guideline for design. Furthermore, and perhaps more importantly, the methodology can be used to *motivate* the development of new manufacturing techniques for FGMs, in particular if the predicted performance of a non-homogeneous composite is substantially better than a homogeneous one.

Acknowledgements

The financial support of the National Science Foundation through grant CMS99-84793 is gratefully acknowledged.

Appendix A. Isotropic normalized properties, bounds and FGM model

Normalized and non-dimensional quantities. In the present analysis, it is useful to work with non-dimensional quantities that can be readily compared since proper scaling is particularly important in the definition of the objective functional. In this appendix, unless otherwise indicated, an *overbar* indicates a *dimensional* quantity whereas a symbol without an overbar refers to a non-dimensional quantity. In order to determine a useful scaling, a brief review of the governing equations is helpful.

Assuming no heat source terms, the local balance of energy in a thermoelastic process is

$$\operatorname{div}\overline{\boldsymbol{q}} = \overline{\rho}\dot{\overline{\eta}}\overline{\theta},$$

where $\overline{\rho}\dot{\overline{\eta}}\overline{\theta} = \overline{\boldsymbol{M}}\cdot\dot{\boldsymbol{\epsilon}}\overline{\theta} + \overline{\rho}\overline{c}\dot{\overline{\theta}}$. It is assumed that the process analyzed is *quasi-static* in the following sense: assume that $|\overline{\boldsymbol{M}}\cdot\dot{\boldsymbol{\epsilon}}\overline{\theta}| \ll |\overline{\rho}\overline{c}\dot{\overline{\theta}}|$. For the isotropic case, the assumption is

$$\frac{\operatorname{tr}\dot{\boldsymbol{\epsilon}}}{\dot{\overline{\theta}}/\overline{\theta}} \ll \frac{1}{G},$$

where $G := \overline{m}/\overline{\rho}\overline{c}$ is the Grüneisen coefficient. For the materials considered here, the Grüneisen coefficient is of the order of magnitude of 1. If the strain rate is of the order of magnitude of $\overline{\alpha}\dot{\overline{\theta}}$, then the previous assumption will hold if $\overline{\alpha}$ is small, which is typically the case. Under this assumption, the balance of energy is uncoupled from the balance of linear momentum.

One can introduce an arbitrary macroscopic length scale $\overline{l}$ related to the region Ω where the analysis is performed. Non-dimensional position vectors are defined as $\boldsymbol{x} = \overline{\boldsymbol{x}}/\overline{l}$. Furthermore, let $\overline{k}_{\max} = \max\{\overline{k}_1, \overline{k}_2\}$ be the largest conductivity of the two design materials and introduce

$$\overline{\beta} := \overline{\rho}\,\overline{c} \quad \text{and} \quad \overline{\beta}_{\max} = \max\{\overline{\beta}_1, \overline{\beta}_2\}, \quad \text{where } \overline{\beta}_i = \overline{\rho}_i\overline{c}_i,\ i = 1, 2.$$

A thermal time scale can be defined as follows: $\overline{t}_{\mathrm{T}} = (\overline{\beta}_{\max}\overline{l}^2)/\overline{k}_{\max}$. It is assumed that a mechanical time scale $\overline{t}_{\mathrm{M}}$ (defined in terms of $\overline{l}$ and a wave speed) and the thermal time scale satisfy $\overline{t}_{\mathrm{M}} \ll \overline{t}_{\mathrm{T}}$. Clearly, a smaller thermal time is obtained using $\overline{\beta}_{\min}$ instead of $\overline{\beta}_{\max}$. However, it is assumed that even if $\overline{\beta}_{\min}$ is used in the definition $\overline{t}_{\mathrm{T}}$, the thermal time scale is larger than the mechanical time scale.

It is assumed that mechanical inertial effects and time fluctuations of mechanical quantities are negligible after time-average in the larger time scale. Since the thermal time scale dominates the quasi-static process, a non-dimensional time t is defined as $t := \overline{t}/\overline{t}_{\mathrm{T}}$. Furthermore, in view of introducing non-dimensional equations, it is convenient to normalize the properties. Let

$$\overline{e}_{\max} = \max\{3\overline{\kappa}_1, 3\overline{\kappa}_2, 2\overline{\mu}_1, 2\overline{\mu}_2\},$$
$$\overline{\alpha}_{\max} = \max\{\overline{\alpha}_1, \overline{\alpha}_2\}.$$

Normalized properties, expressed without an over bar, are defined as

$$e_b := \frac{\overline{e}_b}{\overline{e}_{\max}}, \quad e_s := \frac{\overline{e}_s}{\overline{e}_{\max}}, \quad \alpha := \frac{\overline{\alpha}}{\overline{\alpha}_{\max}}, \quad k := \frac{\overline{k}}{\overline{k}_{\max}}, \quad \beta := \frac{\overline{\beta}}{\overline{\beta}_{\max}}.$$

Dimensionless temperatures and stresses are defined as follows:

$$\theta := \overline{\alpha}_{\max}\overline{\theta}, \quad \boldsymbol{\sigma} := \frac{1}{\overline{e}_{\max}}\overline{\boldsymbol{\sigma}}.$$

The definition of the non-dimensional temperature is motivated by the previous assumption on strain rates, which also motivates the definition of the non-dimensional stress. Prescribed displacements are normalized by $\overline{l}$, tractions by $\overline{e}_{\max}$, heat fluxes by $\overline{k}_{\max}/(\overline{\alpha}_{\max}\overline{l}^2)$ and film coefficients by $\overline{k}_{\max}/\overline{l}$.

FGM model. For isotropic conductivity, the Hashin–Shtrikman–Walpole bounds are shown in Fig. 9 (left) for different values of the ratio of normalized conductivites $r = k_2/k_1$, where it is assumed that $k_2 \leqslant k_1 = 1$. Fig. 9 (right) shows the maximum difference between the upper and lower bounds as a function of r. As shown in Fig. 9 (right), the difference between the upper and lower bounds decreases rapidly as a function of r. The same situation occurs for other properties such as bulk and shear moduli, as shown in Figs. 10–12. If one assumes that a two-phase FGM is macroscopically isotropic, then for relatively large values of r, its effective properties can be well approximated by, e.g., the average between the upper and lower bounds. To illustrate this assertion, consider a Ni/alumina composite. At room temperature, the properties are shown in Table 4. It is important to observe, however, that these properties depend on the reference temperature (room temperature in this case). For large temperature excursions, this dependence needs to be taken into account. However, this falls outside of the scope of the present work.

For the term $\beta = \rho c$, it is assumed that it can be approximated by an monotonic expression of the form

$$\beta(\omega) = \omega^p(\beta_1 - \beta_2) + \beta_2, \tag{A.1}$$

p being a constant power. Observe that if one uses a simple linear interpolation for the density and the specific heat and if these properties are not ordered (i.e., $(\overline{\rho}_1 - \overline{\rho}_2)(\overline{c}_1 - \overline{c}_2) \leqslant 0$) then the product β is *not* a monotonic function of volume fraction. Such case is not considered here.

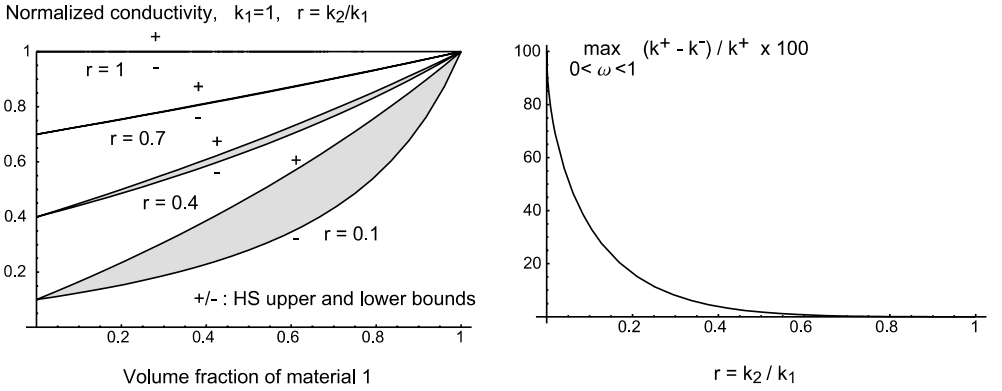

Fig. 9. Left: upper and lower Hashin–Shtrikman–Walpole bounds of normalized conductivity as a function of volume fraction ω for various values of $r = k_2/k_1$. Right: maximum difference between upper and lower bounds for conductivity as a function of $r = k_2/k_1$.

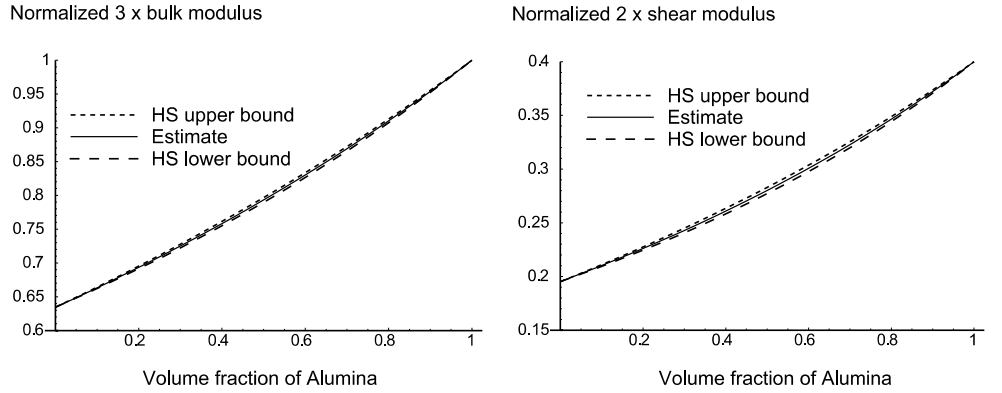

Fig. 10. For Ni/Al_2O_3, normalized 3 × bulk modulus (left) and normalized 2 × shear modulus (right) as a function of volume fraction of Al_2O_3.

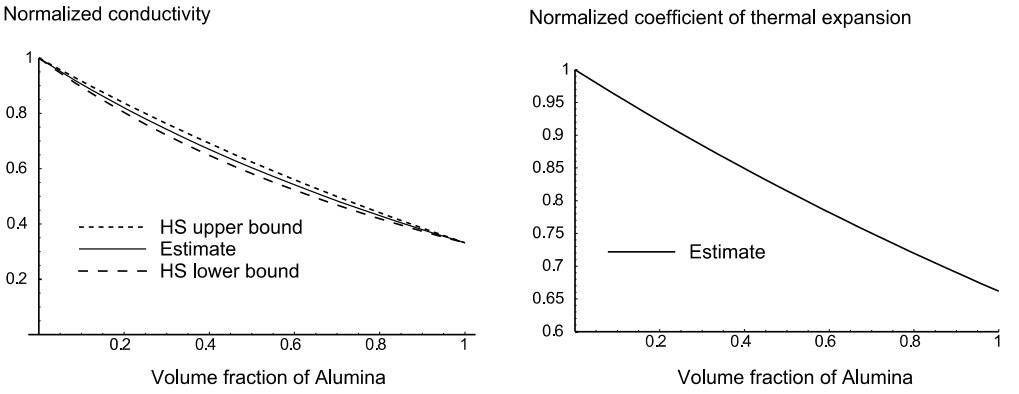

Fig. 11. For Ni/Al_2O_3, normalized conductivity (left) and normalized coefficient of thermal expansion (right) as a function of volume fraction of Al_2O_3. The estimate for the coefficient of thermal expansion is based on the estimate for the bulk modulus shown in Fig. 10.

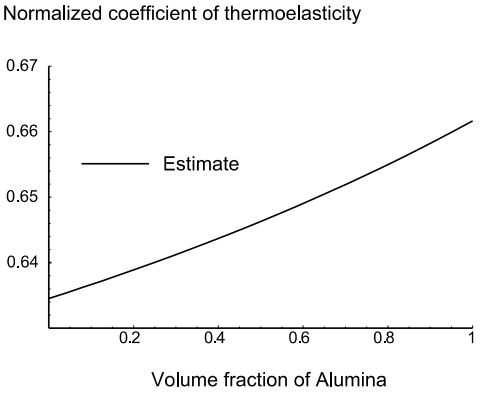

Fig. 12. For Ni/Al_2O_3, normalized coefficient of thermoelasticity $m = 3\kappa\alpha$ as a function of volume fraction of Al_2O_3.

Table 4
Properties of Ni and alumina at room temperature

Property at room temperature	Alumina	Ni
Bulk, κ (Pa)	2.62×10^{11}	1.66×10^{11}
Shear, μ (Pa)	1.57×10^{11}	7.67×10^{10}
Coefficient of thermal expansion, α (K^{-1})	8.8×10^{-6}	13.3×10^{-6}
Conductivity, k ($W\,m^{-1}\,K^{-1}$)	3.01×10^{1}	9.07×10^{1}
Specific heat, c ($J\,kg^{-1}\,K^{-1}$)	7.75×10^{2}	4.44×10^{2}
Density, ρ ($kg\,m^{-3}$)	3.97×10^{3}	8.9×10^{3}

Appendix B. The macroscopically isotropic, plane stress, plane flux case

An important special case is when the forward (direct) problem (P) corresponds to plane stress, plane flux and the FGM is macroscopically isotropic. The underlying assumption is that the domain corresponds to, e.g., a thin plate with zero flux and no tractions applied on the top and bottom and all other loads are applied in the same plane as the plate. It is assumed that the composition of the FGM is the same in the thickness direction. In that case, observe that $\boldsymbol{M} \cdot \boldsymbol{\epsilon}^* = 3\kappa\alpha \operatorname{tr} \boldsymbol{\epsilon}^* = \alpha \operatorname{tr} \boldsymbol{\sigma}^*$. For the plane stress case, one has to specify a stress target that is consistent with the plane stress assumption, i.e., the stress target has to satisfy $\breve{\sigma}_{i3} \equiv 0$ for $i = 1, 2, 3$, where 3 corresponds to the normal of the plane with respect to which the stresses are assumed to be zero. The adjoint mechanical problem can be taken as a plane stress problem as well, hence the total adjoint strain component $\epsilon^*_{\mathrm{tot},33}$ has to accommodate the stress-free top and bottom surfaces. This is important since the gradient (12) includes contributions from both ϵ_{33} and $\epsilon^*_{\mathrm{tot},33} = \epsilon^*_{33}$, where

$$\epsilon_{33} = -\frac{\lambda}{\lambda + 2\mu} \operatorname{tr} \boldsymbol{\epsilon}_p + \frac{m}{\lambda + 2\mu}(\theta - \theta_{\mathrm{r}})$$

and

$$\epsilon^*_{33} = -\frac{\lambda}{\lambda + 2\mu} \operatorname{tr}\left(\boldsymbol{\epsilon}^*_{\mathrm{tot},p} - \xi^{\mathrm{s}}(\mathbf{A}\boldsymbol{e})_p\right),$$

where $\lambda = \kappa - (2/3)\mu$ is the first Lamé modulus, tr is the trace, and the subscript p represents the in-plane restrictions of the corresponding tensors. In view of (12) and the previous relations, the first term in the gradient, for the plane stress and isotropic FGM case, can be computed as follows:

$$\boldsymbol{\epsilon}^* \cdot [\mathbf{C}_\omega \boldsymbol{\epsilon} - \boldsymbol{M}_\omega(\theta - \theta_r)] = \boldsymbol{\epsilon}_p^* \cdot \left[\mathbf{C}_\omega^p \boldsymbol{\epsilon}_p - \boldsymbol{M}_\omega^p(\theta - \theta_r)\right], \tag{B.1}$$

where

$$\mathbf{C}^p = (3p\kappa)\mathbf{H}_p + 2\mu\mathbf{J}_p, \quad \boldsymbol{M}^p = (pm)\boldsymbol{I}_p, \quad \mathbf{H}_p = \tfrac{1}{2}\boldsymbol{I}_p \otimes \boldsymbol{I}_p, \quad \mathbf{J}_p = \mathbf{I}_p - \mathbf{H}_p. \tag{B.2}$$

In (B.2), $\boldsymbol{I}_p$ and $\mathbf{I}_p$ are the in-plane restrictions of the second and fourth order (symmetric) identity tensors respectively and the plane stress factor p is $p = 2\mu/(\kappa + (4/3)\mu)$. A relevant consequence of (B.1) and (B.2) is that for the sensitivity analysis (i.e., local changes in material properties with respect to volume fractions ω), the derivatives of the modified bulk modulus $3p\kappa$ and of the modified thermoelastic modulus pm need to take into account the derivative of p with respect to ω which, in turn, includes derivatives of κ and μ.

References

Bendsøe, M.P., 1995. Optimization of structural topology, shape, and material. Springer, Berlin.

Carthel, C., Glowinski, R., Lions, J.L., 1994. On exact and approximate boundary controllabilities for the heat-equation-a numerical approach. J. Opt. Theo. App. 82 (3), 429–484.

Cherkaev, A., 1999. Variational Methods for Structural Optimization. Springer-Verlag, Berlin.

Dems, K., Mróz, Z., 1998. Methods of sensitivity analysis. In: Kleiber, M. (Ed.), Handbook of Computational Solid Mechanics: Survey and Comparison of Contemporary Methods. Springer, Berlin.

Drugan, W.J., Willis, J.R., 1996. A micromechanics-based nonlocal constitutive equation and estimates of representative volume element size for elastic composites. J. Mech. Phys. Solids 44, 497–524.

Hashin, Z., Shtrikman, S., 1963. A variational approach to the theory of the elastic behaviour of multiphase materials. J. Mech. Phys. Solids 11, 127–140.

Lipton, R., 2002a. Design of functionally graded composites in the presence of stress constraints, Int. J. Sol. Struct., in press.

Lipton, R., 2002b. Relaxation through homogenization for optimal design problems with gradient constraints, J. Opt. Theory Appl., in press.

Suresh, S., Mortensen, A., 1998. Fundamentals of functionally graded materials: processing and thermomechanical behaviour of graded metals and metal-ceramic composites. IOM Communications.

Tanaka, K., Watanabe, H., Sugano, Y., Poterasu, V.F., 1996. A multicriterial material tailoring of a hollow cylinder in functionally gradient materials: Scheme to global reduction of thermoelastic stresses. Comp. Meth. App. Mech. Eng. 135 (3–4), 369–380.

Tortorelli, D.A., Haber, R.B., 1989. First-order design sensitivities for transient conduction problems by an adjoint method. Int. J. Num. Meth. Eng. 28 (4), 733–752.

Turteltaub, S., 2002. Functionally graded materials for prescribed field evolution. Comp. Meth. App. Mech. Eng. 191 (21–22), 2283–2296.